On the Application of the Microgenetic Algorithm to the Design of Broad-Band Microwave Absorbers Comprising Frequency-Selective Surfaces Embedded in Multilayered Dielectric Media

Sourav Chakravarty, *Student Member, IEEE*, Raj Mittra, *Life Fellow, IEEE*, and Neil Rhodes Williams, *Member, IEEE*

***Abstract*—In this paper, we present a procedure for synthesizing broad-band microwave absorbers incorporating frequency-selective surface (FSS) screens embedded in dielectric media using a binary coded genetic algorithm (GA) [1], [2]. The GA simultaneously and optimally chooses the material in each layer, thickness of each layer, FSS screen periodicity in the x- and y-directions, its placement within the dielectric composite, and the FSS screen material. Additionally, the GA generates the cell structure of the FSS screen. The result is a multilayer composite that provides maximum absorption of both TE and TM waves for a prescribed range of frequencies and incident angles. This technique automatically places an upper bound on the total thickness of the composite.**

***Index Terms*—Frequency-selective surfaces, genetic algorithm, microgenetic algorithm, microwave absorbers, multilayer dielectrics.**

I. Introduction

GENETIC algorithms (GAs) fall under a special category of optimization schemes that are robust stochastic search methods modeled on the principles of natural selection. The powerful heuristic of the GA as an optimizer is useful for solving complex combinatorial problems. It is particularly effective in searching for global maxima in a multidimensional and multimodal function domain. The GA excels when the problem can be cast in a combinatorial form. It simultaneously processes a population of points in the optimization space, and use stochastic operators to transition from one generation of points to the next, resulting in a decreased probability of them being trapped in local extremes.

In this paper, the GA is employed to solve a computationally intensive design problem. In the past, GAs have met with minimal success in solving these problems within a practical time frame. A design problem is typically categorized as computationally intensive when a single function evaluation takes a significant amount of computation time. The problem dealt with in this paper partly involves the analysis of scattering from FSS screens, which is achieved using the method of moments (MoM). The main contributors to the large computation time for a single function evaluation are the fill time and inversion of the matrix inherent to the MoM, which are dependent on the complexity of the FSS screen design. The number of function evaluations in a single generation depends on the population base used for the optimization. For conventional GAs, sizing the population is problem specific and a strong function of the length and cardinality of the chromosome [3], [6]. For most optimization problems, the length of the chromosome is a function of the number of parameters to be optimized, the individual parameter range, and the step size to be implemented. Hence, for a multidimensional search space, a large population base and several generations is required to achieve optimal or near-optimal results if the conventional GA is used, and this places a considerable burden on computational time and resources. One possible approach to solving this type of problem would be to employ a parallel implementation of the GA. However, in this paper, we avoid the complexity of parallel-GA implementation and solve the problem efficiently by using a serially implemented version referred to as the microgenetic algorithm (MGA).

It is well known that conventional serial GAs perform poorly with small population sizes due to insufficient information processing and they converge prematurely to nonoptimal results. To circumvent this difficulty, a serially implemented GA with a small population base and efficient convergence properties is required. Goldberg [4] has suggested that the key to success with small population sizes is to use the MGA. We follow this suggestion and employ the above algorithm to optimize the problem at hand.

The MGA has the following two major advantages: 1) small population base for each generation and 2) it reaches near-optimal regions quicker than the conventional GAs that deal with a large population base. The general choice of population size for conventional GAs can range from 100 to 10000, while the MGAs typically work with a population size from 20 to 50. Numerical experiments show that using the MGA can decrease the computational run time by 50%, even for "best-case" problems for the conventional GAs.

The outline for the remainder of this paper is as follows. Section II describes the basic MGA algorithm and the process of

Manuscript received September 21, 2000.

S. Chakravarty and R. Mittra are with the Electromagnetic Communication Laboratory, Pennsylvania State University, University Park, PA 16802 USA.

N. R. Williams is with Advanced Electromagnetic Products, W. L. Gore and Associates, Newark, DE 19714-9236 USA.

Publisher Item Identifier S 0018-9480(01)03985-0.

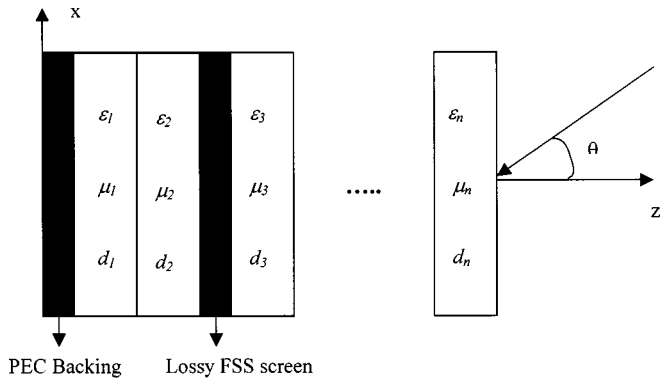

Fig. 1. FSS screen embedded in multilayered dielectric composite.

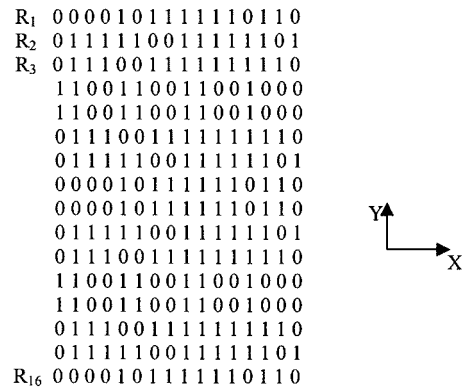

Fig. 2. FSS cell structure.

coding the parameters. Section III presents the MoM analysis in the spectral domain, employed to compute the currents on the FSS screen. Numerical results are discussed in Section IV. Finally, some conclusions that are based on the results of the numerical experiments are drawn in Section V.

II. GA Formulation

Fig. 1 shows a multilayered composite structure whose parameters we wish to optimize with a view to realizing a specified frequency response. Assume that we are given a set of different materials M_m with frequency-dependent permittivities $\varepsilon_i(f)\,(i = 1, \ldots M_m)$. The design goal is to determine a coating consisting of N different layers, an FSS cell design generated by the GA, the FSS cell periodicity, its position within the dielectric composite, and the FSS screen material, such that the coating exhibits a low reflection coefficient for a prescribed set of frequencies $f_i\,(i = 1, \ldots, F_f)$ and incident angles $\theta_i\,(i = 1, \ldots, A_\theta)$ for both the TE and TM polarizations. In the context of the present problem, the magnitude of the largest reflection coefficient is minimized for a set of angles, for both TE and TM polarizations, and for a selected band of frequencies. Hence, the fitness function can be written as

$$F\left(m_1, d_1, \ldots, m_N, d_N, S_{\text{des}}, t_x, t_y, S_{\text{pos}}\right) = -\max_{ij}\left\{\Gamma^{TE/TM}\left(\theta_i, f_j\right)\right\} \quad (1)$$

where m_i and d_i are the material parameter and thickness of the ith layer, respectively, S_{des} is the unit cell of the periodic FSS screen generated by the GA, t_x and t_y are the x- and y-periodicities of the FSS screen, S_{pos} is the position of the FSS screen within the dielectric composite, and $\Gamma^{TE/TM}(\theta_i, f_j)$ is the reflection coefficient, which is a function of polarization, incident angle, and frequency.

The GA operates on a coding of the parameters. The coded representation of the coating consists of sequence of bits that contain information regarding each parameter. Each parameter is represented by a string of bits, and the length of each string is determined by the allowed range of real values and the discretization step to be implemented. The entire composite that follows can be represented by the sequence C, and is referred to as a chromosome:

$$C = L_1, \ldots, L_N D_1, \ldots, D_N (CL)_1, \ldots, (CL)_N \times T_x T_y P (FLR)(FLI)(CS)(CD)_1, \ldots, (CD)_j \quad (2)$$

where, e.g., given a database containing $M_m = 2^{M_{mb}}$ different materials, the material choice for the ith layer is represented by a sequence L_i of M_{mb} bits as

$$L_i = l_i^1 l_i^2, \ldots, l_i^{M_{mb}}. \quad (3)$$

Similarly, in (2), D_i is a sequence of M_{db} bits, representing the thickness of the ith layer, and T_x and T_y are strings of length $M_{t_x b}$ and $M_{t_v b}$, representing the x- and y-periodicities of the FSS screen. The string P consists of 2 bits representing the position of the FSS screen in the composite, CL_i and CS are strings of unit length that represent the choice of selecting a lossy or lossless dielectric for the ith layer and lossy or PEC material for the FSS screen, respectively, and FLR and FLI are strings of length M_{flrb} and M_{flib} that represent the real and imaginary parts of the FSS surface impedance. The formation of sequence CD_i is explained below in more detail.

The GA designs the FSS cell structure automatically. The part of the code that analyzes the FSS screen embedded in dielectric media accepts a 16 × 16 discretization (32 × 32 and 64 × 64 discretizations can also be handled) of the periodic structure unit cell in the form of 1's (ones) and 0's (zeros); the 1's corresponding to the perfect electric conductor (PEC) or lossy metal and the 0's corresponding to free space. The GA randomly generates this 16 × 16 gridded structure filled with 1's and 0's, as explained below. Fig. 2 shows a 16 × 16 matrix filled with 1's and 0's.

The GA considers each row in the FSS cell as a parameter. For each row, the GA generates a random number from 0 to $2^{M_{cb}} - 1$, where M_{cb} is the number of columns in the FSS cell matrix. These random numbers are then converted to binary format for each row. These binary numbers are combined into an array, which is ready to be analyzed by the FSS code. Symmetry is introduced into the FSS structure by making rows 5–8 the mirror image of rows 1–4 and rows 9–16 the mirror image of rows 1–8. This reduces the effective number of GA parameters needed to design the FSS cell from 16 to 4, resulting in efficient optimization. Thus, the FSS cell can be designed by discretizing each row into a sequence $(CD)_j$ of M_{cb} bits as

$$(CD)_j = (CD)_j^1 (CD)_j^2, \ldots, (CD)_j^{M_{cb}} \quad (4)$$

where j is the number of rows considered by the GA as parameters and $j_{\max}$ is the total number of rows in the FSS cell structure. Each sequence in (2) consists of $(2 + M_{mb} + M_{db} + M_{txb} + M_{tyb} + 2 + j * M_{cb} + M_{flrb} + M_{flib})$ bits.

The GA, which optimally chooses each parameter, is an iterative optimization procedure, which starts with a randomly selected population of potential solutions, and gradually evolves toward improved solutions via the application of the genetic operators. These genetic operators mimic the processes of procreation in nature. The GA begins with a large population P_0, comprising an aggregate of sequences, with each sequence [similar to the one represented in (2)], consisting of a randomly selected string of bits. It then proceeds to iteratively generate a new population P_{i+1}, derived from P_i, by the application of selection, crossover, and mutation operators.

For this particular problem, a variant of the conventional GA, i.e., the MGA, was used. It has been shown that MGAs avoid premature convergence and show faster convergence to the near-optimal region compared to the conventional GA for multidimensional multimodal problems [4], [5]. The MGA starts with a random and small population. The population evolves in conventional GA fashion and converges in a few generations (typically, 4–5). At this point, keeping the best individual from the previously converged generations, a new random population is chosen and the evolution process restarts. In our case, population convergence occurs when the difference in bits between the best and other individuals is less than 5%.

Among the many types of selection strategies that can be used to suit a particular application, the one used for the present problem was the tournament selection. In this method, a sub-population of N individuals is randomly chosen from the population. The individuals of this sub-population compete on the basis of their fitness. The individual in the sub-population with the highest fitness value wins the tournament, thus becoming the selected individual. Members of the entire sub-population are then put back into the general population and the process is repeated. This selection was preferred because it converges more rapidly and it has a faster execution time than many other competing schemes [7].

Once a pair of individuals is selected as parents, the basic crossover operator creates an offspring by recombining the chromosomes of its parents. The mutation operator was not utilized in our problem, i.e., $p_{\text{mut}} = 0$. Uniform crossover was preferred to single point crossover, as it has been found that MGA convergence is faster with the uniform crossover [5], [6]. The value of $p_{\text{cross}} = 0.5$ was used. Elitism [8] was also used.

III. Frequency-Selective-Surface Scattering Formulation

In this section, we consider the formulation of scattering from a frequency-selective surface (FSS) in the spectral domain. As the objective of this paper is to show a successful GA implementation using the FSS, only the basic formulation will be given here. For further details, the reader is referred to [9]–[12]. A general full-wave analysis for a plane wave incident at any arbitrary angle is formulated. The spectral-domain workspace converts the convolution form of the integral equation into an algebraic one, resulting in a highly simplified approach. The integral equation is solved using Galerkin's method applied directly in the spectral domain.

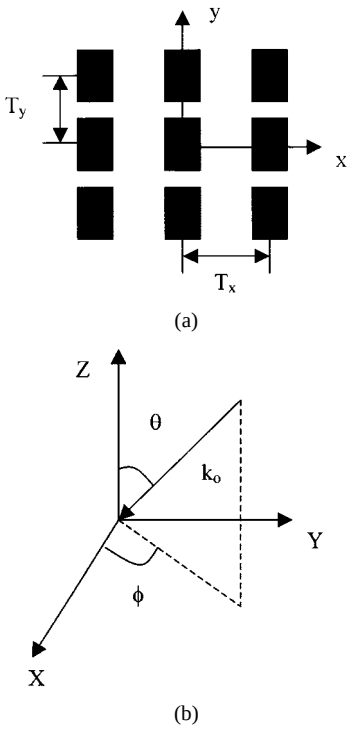

Fig. 3. (a) Periodic FSS screen. (b) Uniform plane wave propagating in the k_0 direction incident on a freestanding FSS screen.

We initially consider the geometry of a freestanding FSS, shown in Fig. 3(a). Let $\vec{J}$ be the current induced on the FSS surface due to a given incident field, as shown in Fig. 3(b), and let $\vec{A}$ be the magnetic vector potential due to this current $\vec{J}$. At the $z = 0$ plane with the time convention $e^{j\omega t}$ suppressed, $\vec{A}$ can be written as

$$\vec{A}(x,y) = \overline{\overline{G}}(x,y) * \vec{J}(x,y) \tag{5}$$

where

$\overline{\overline{G}}(x,y)$	$= \frac{e^{-jk_0 r}}{4\pi r}\overline{\overline{I}}$;
r	$= \sqrt{x^2+y^2}$;
k_0	free-space wavenumber;
$\overline{\overline{I}}$	identity tensor;
$*$	convolution operator.

From $\vec{A}$, the scattered electric field can be derived as

$$\begin{bmatrix} E_x^s \\ E_y^s \end{bmatrix} = \frac{1}{j\omega\varepsilon_0} \begin{bmatrix} \frac{\partial^2}{\partial x^2} + k_0^2 & \frac{\partial^2}{\partial x \partial y} \\ \frac{\partial^2}{\partial x \partial y} & \frac{\partial^2}{\partial y^2} + k_0^2 \end{bmatrix} \begin{bmatrix} A_x \\ A_y \end{bmatrix} \tag{6}$$

expressing (6) in the spectral domain by taking the Fourier transform, we get

$$\begin{bmatrix} \tilde{E}_x^s(\alpha,\beta) \\ \tilde{E}_y^s(\alpha,\beta) \end{bmatrix} = \frac{1}{j\omega\varepsilon_0} \begin{bmatrix} k_0^2 - \alpha^2 & -\alpha\beta \\ -\alpha\beta & k_0^2 - \beta^2 \end{bmatrix} \begin{bmatrix} \tilde{A}_x(\alpha,\beta) \\ \tilde{A}_y(\alpha,\beta) \end{bmatrix}. \tag{7}$$

Repeating the procedure above for (5), we get

$$\begin{bmatrix} \tilde{A}_x(\alpha,\beta) \\ \tilde{A}_y(\alpha,\beta) \end{bmatrix} = \tilde{\overline{\overline{G}}}(\alpha,\beta) \begin{bmatrix} \tilde{J}_x(\alpha,\beta) \\ \tilde{J}_y(\alpha,\beta) \end{bmatrix} \tag{8}$$

where

$$\tilde{\overline{\overline{G}}}(\alpha,\beta)=\frac{-j}{2(k_0^2-\alpha^2-\beta^2)^{1/2}}\tilde{\overline{\overline{I}}}$$

and α and β are the transform variables corresponding to the x and y coordinates, respectively. Substituting (8) into (7), we express the transform of the scattered electric fields in terms of the unknown current density in the spectral domain as

$$\begin{bmatrix}\tilde{E}_x^s(\alpha,\beta)\\ \tilde{E}_y^s(\alpha,\beta)\end{bmatrix}=\frac{1}{j\omega\varepsilon_0}\begin{bmatrix}k_0^2-\alpha^2 & -\alpha\beta\\ -\alpha\beta & k_0^2-\beta^2\end{bmatrix}\times\tilde{\overline{\overline{G}}}(\alpha,\beta)\begin{bmatrix}\tilde{J}_x(\alpha,\beta)\\ \tilde{J}_y(\alpha,\beta)\end{bmatrix}. \quad (9)$$

Since the structure is periodic, the current density components $J_x(x,y)$ and $J_y(x,y)$ have discrete spectrums in the spectral domain, i.e., $\tilde{J}_x(\alpha,\beta)$ and $\tilde{J}_y(\alpha,\beta)$ are nonzero for discrete values of α and β, *viz.*, α_m and β_n, which correspond to the Floquet harmonics. α_m and β_n can be expressed as

$$\alpha_m=\frac{2\pi m}{T_x}+k_0\sin\theta\cos\phi$$
$$\beta_n=\frac{2\pi n}{T_y}+k_0\sin\theta\sin\phi.$$

Taking the inverse transform of (9) and applying the boundary condition $\vec{E}^s=-\vec{E}^i$ on the conducting surfaces of the FSS, we get

$$\frac{1}{j\omega\varepsilon_0}\sum_m\sum_n\begin{bmatrix}k_0^2-\alpha_m^2 & -\alpha_m\beta_n\\ -\alpha_m\beta_n & k_0^2-\beta_n^2\end{bmatrix}\tilde{\overline{\overline{G}}}(\alpha_m,\beta_n)\times\begin{bmatrix}\tilde{J}_x(\alpha_m,\beta_n)\\ \tilde{J}_y(\alpha_m,\beta_n)\end{bmatrix}\exp\Big[j(\alpha_m x+\beta_n y)\Big]=-\begin{bmatrix}E_x^i(x,y)\\ E_y^i(x,y)\end{bmatrix}. \quad (10)$$

Equation (10) can now be solved using Galerkin's procedure for the unknown currents that are expressed in terms of subdomain basis functions (rooftops) $\vec{g}_i$ as

$$\vec{J}=\sum_i U_i\vec{g}_i \quad (11)$$

where U_i are the unknown coefficients to be determined. Substituting (11) into (10) and using $\vec{g}_i$ as testing functions, (10) is transformed into a matrix equation [12] that is solved to obtain the values of U_i. The values of the induced currents are obtained from (11) once U_i are known.

For a finite surface conductivity, the total electric field no longer vanishes on the surface of the screen, and it becomes necessary to modify (10) to satisfy the impedance type boundary condition, which is expressed as follows:

$$\begin{bmatrix}E_x^s\\ E_y^s\end{bmatrix}+\begin{bmatrix}E_x^i\\ E_y^i\end{bmatrix}=Z_s\begin{bmatrix}J_x\\ J_y\end{bmatrix} \quad (12)$$

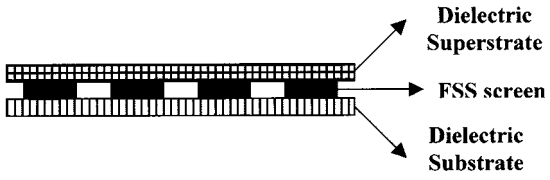

Fig. 4. FSS screen embedded in dielectric layers.

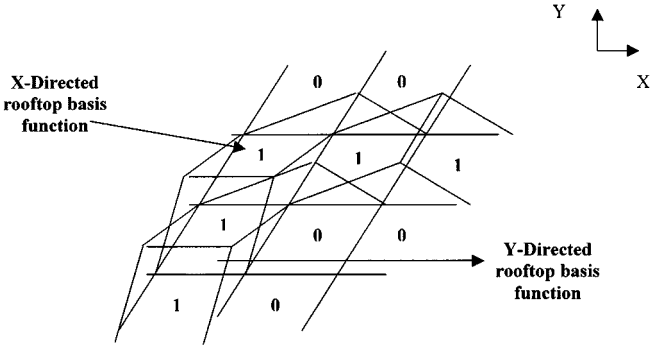

Fig. 5. Basis function assignment for part of a FSS cell.

where Z_s is the sheet impedance of an infinitesimally thin FSS screen. Using (12), (10) is modified as

$$\frac{1}{j\omega\varepsilon_0}\sum_m\sum_n\begin{bmatrix}k_0^2-\alpha_m^2 & -\alpha_m\beta_n\\ -\alpha_m\beta_n & k_0^2-\beta_n^2\end{bmatrix}\tilde{\overline{\overline{G}}}(\alpha_m,\beta_n)\times\begin{bmatrix}\tilde{J}_x(\alpha_m,\beta_n)\\ \tilde{J}_y(\alpha_m,\beta_n)\end{bmatrix}\exp\Big[j(\alpha_m x+\beta_n y)\Big]-Z_s\begin{bmatrix}J_x\\ J_y\end{bmatrix}=-\begin{bmatrix}E_x^i(x,y)\\ E_y^i(x,y)\end{bmatrix}. \quad (13)$$

The extension of the formulation given above to the case of an FSS structure with a dielectric superstrate and a substrate, as shown in Fig. 4, can be done by simply replacing the spectral dyadic Green's function in (10) and (13) with a composite Green's function, which accounts for the presence of both the superstrate and substrate. Since such a composite Green's function for layered dielectric media can be easily found in the literature [9], [12], [13], the details shall not be provided here. Replacing the spectral dyadic Green's function with the composite Green's function in (10) and (13), we get

$$\frac{1}{j\omega\varepsilon_0}\sum_m\sum_n\begin{bmatrix}k_0^2-\alpha_m^2 & -\alpha_m\beta_n\\ -\alpha_m\beta_n & k_0^2-\beta_n^2\end{bmatrix}\tilde{\overline{\overline{G}}}''(\alpha_m,\beta_n)\times\begin{bmatrix}\tilde{J}_x(\alpha_m,\beta_n)\\ \tilde{J}_y(\alpha_m,\beta_n)\end{bmatrix}\exp\Big[j(\alpha_m x+\beta_n y)\Big]=-\begin{bmatrix}E_x^i(x,y)\\ E_y^i(x,y)\end{bmatrix} \quad (14)$$

$$\frac{1}{j\omega\varepsilon_0}\sum_m\sum_n\begin{bmatrix}k_0^2-\alpha_m^2 & -\alpha_m\beta_n\\ -\alpha_m\beta_n & k_0^2-\beta_n^2\end{bmatrix}\tilde{\overline{\overline{G}}}''(\alpha_m,\beta_n)\times\begin{bmatrix}\tilde{J}_x(\alpha_m,\beta_n)\\ \tilde{J}_y(\alpha_m,\beta_n)\end{bmatrix}\exp\Big[j(\alpha_m x+\beta_n y)\Big]-Z_s\begin{bmatrix}J_x\\ J_y\end{bmatrix}=-\begin{bmatrix}E_x^i(x,y)\\ E_y^i(x,y)\end{bmatrix} \quad (15)$$

where $\tilde{\overline{\overline{G}}}''(\alpha_m,\beta_n)=$ composite spectral dyadic Green's function for layered dielectric media.

TABLE I
MEASURED VALUES OF REAL ε_r AS A FUNCTION OF FREQUENCY

Material type	Type 1	Type 3	Type 5	Type 7	Type 9	Type 11	Type 13	Type 15	Type 17	Type 19
F (GHz)										
19.0	4.48257	5.21093	5.83968	7.08171	22.41061	9.83625	11.86623	12.73006	17.96287	24.76098
20.0	4.48299	5.21152	5.84028	7.08190	22.43457	9.83703	11.86821	12.73291	17.96867	24.76884
21.0	4.48331	5.21190	5.84070	7.08231	22.44027	9.83769	11.86921	12.73412	17.97069	24.77163
22.0	4.48353	5.21216	5.84098	7.08264	22.44174	9.83816	11.86979	12.73477	17.97164	24.77292
23.0	4.48367	5.21232	5.84117	7.08288	22.44219	9.83848	11.87017	12.73516	17.97217	24.77365
24.0	4.48377	5.21244	5.84130	7.08304	22.44237	9.83870	11.87041	12.73541	17.97249	24.77411
25.0	4.48383	5.21251	5.84138	7.08314	22.44247	9.83884	11.87057	12.73557	17.97271	24.77440
26.0	4.48388	5.21256	5.84143	7.08321	22.44252	9.83893	11.87068	12.73568	17.97285	24.77459
27.0	4.48390	5.21259	5.84147	7.08326	22.44256	9.83899	11.87075	12.73575	17.97295	24.77473
28.0	4.48392	5.21261	5.84149	7.08329	22.44258	9.83904	11.87080	12.73580	17.97300	24.77481
29.0	4.48393	5.21262	5.84151	7.08331	22.44260	9.83906	11.87083	12.73583	17.97305	24.77487
30.0	4.48394	5.21263	5.84152	7.08333	22.44261	9.83908	11.87085	12.73585	17.97308	24.77491
31.0	4.48395	5.21264	5.84153	7.08334	22.44262	9.83909	11.87086	12.73586	17.97309	24.77493
32.0	4.48395	5.21265	5.84153	7.08334	22.44262	9.83910	11.87087	12.73587	17.97310	24.77495
33.0	4.48395	5.21265	5.84154	7.08334	22.44262	9.83911	11.87088	12.73588	17.97311	24.77497
34.0	4.48396	5.21265	5.84154	7.08335	22.44263	9.83911	11.87088	12.73588	17.97312	24.77497
35.0	4.48396	5.21265	5.84154	7.08335	22.44263	9.83912	11.87088	12.73589	17.97312	24.77497
36.0	4.48396	5.21265	5.84154	7.08335	22.44263	9.83912	11.87088	12.73589	17.97312	24.77497

TABLE II
MEASURED VALUES OF IMAGINARY ε_r AS A FUNCTION OF FREQUENCY

Material type	Type 1	Type 3	Type 5	Type 7	Type 9	Type 11	Type 13	Type 15	Type 17	Type 19
F (GHz)										
19.0	1.84577	1.18222	1.65893	2.31634	8.03474	4.98416	9.74786	8.17483	14.62385	19.05948
20.0	1.86013	1.18308	1.65913	2.31605	8.03710	4.96560	9.73054	8.14305	14.59117	19.01088
21.0	1.86536	1.18340	1.65922	2.31597	8.03804	4.95882	9.72429	8.13155	14.57935	18.99331
22.0	1.86726	1.18351	1.65925	2.31595	8.03841	4.95636	9.72205	8.12741	14.57511	18.98702
23.0	1.86794	1.18355	1.65927	2.31594	8.03856	4.95547	9.72125	8.12593	14.57359	18.98477
24.0	1.86819	1.18357	1.65928	2.31594	8.03862	4.95515	9.72097	8.12540	14.57306	18.98397
25.0	1.86828	1.18358	1.65928	2.31594	8.03865	4.95504	9.72087	8.12521	14.57287	18.98369
26.0	1.86831	1.18358	1.65928	2.31594	8.03866	4.95500	9.72084	8.12515	14.57281	18.98359
27.0	1.86832	1.18358	1.65928	2.31594	8.03866	4.95499	9.72083	8.12512	14.57279	18.98356
28.0	1.86833	1.18358	1.65928	2.31594	8.03867	4.95498	9.72082	8.12512	14.57278	18.98355
29.0	1.86833	1.18358	1.65928	2.31594	8.03867	4.95498	9.72082	8.12511	14.57277	18.98354
30.0	1.86833	1.18358	1.65928	2.31594	8.03867	4.95498	9.72082	8.12511	14.57277	18.98354
31.0	1.86833	1.18358	1.65928	2.31594	8.03867	4.95498	9.72082	8.12511	14.57277	18.98354
32.0	1.86833	1.18358	1.65928	2.31595	8.03867	4.95498	9.72082	8.12511	14.57277	18.98354
33.0	1.86833	1.18358	1.65928	2.31595	8.03867	4.95498	9.72082	8.12511	14.57277	18.98354
34.0	1.86833	1.18358	1.65928	2.31595	8.03867	4.95498	9.72082	8.12511	14.57277	18.98354
35.0	1.86833	1.18358	1.65928	2.31595	8.03867	4.95498	9.72082	8.12511	14.57277	18.98354
36.0	1.86833	1.18358	1.65928	2.31595	8.03867	4.95498	9.72082	8.12511	14.57277	18.98354

Each of the 256 locations on the grid generated by the GA is checked by the FSS code. If a particular location and a location to its left- or right-hand sides have 1's, then a rooftop basis function, representing the x-directed current, is assigned across the two locations such that it is centered between them. This is also done between unit cells, i.e., if on any row, columns 1 and 16 are both "1," then a x-directed rooftop basis will be centered on the unit cell boundary, covering column 16 of one unit cell and column 1 of the next unit cell. The above procedure is repeated for the y-directed rooftop basis functions. Fig. 2 shows an FSS cell structure generated using 1's and 0's and Fig. 5 shows how the x- and y-directed rooftop basis functions are assigned.

IV. NUMERICAL RESULTS

The algorithm described in Section II was successfully applied to the synthesis of broad-band microwave absorbers in the frequency range from 19.0 to 36.0 GHz. The number of dielectric layers was fixed at four and was surrounded by air on one side and terminated on the other side by a PEC backing. Though only dielectric layers with electric loss were considered, the method can be further extended to handle both electric and magnetic losses. The measured values of ε_r' and ε_r'' of ten different lossy materials were considered and a database of these values as a function of frequency were created and are shown in Tables I and II, respectively. Linear interpolation was used

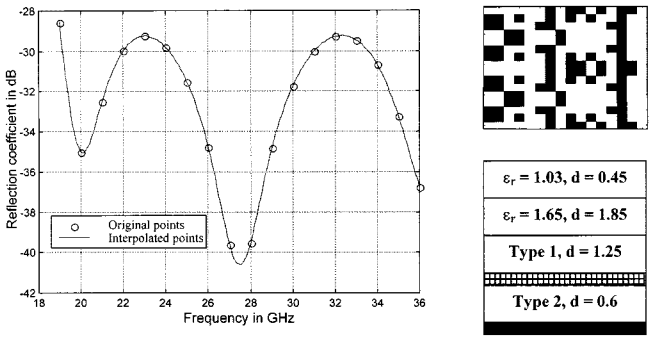

Fig. 6. Normal incidence, TE polarization.

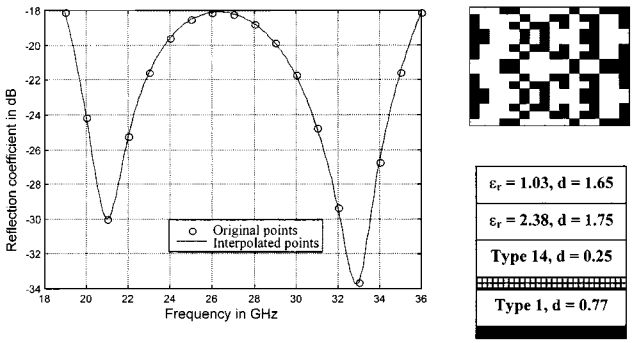

Fig. 7. Oblique incidence ($\theta = 45.0, \phi = 0.0$), TE polarization.

to generate the values of ε_r' and ε_r'' as a function of frequency for intermediate material types; to obtain the values of the real and imaginary parts of permittivity for even-numbered material types at a particular frequency, the odd-numbered material types were averaged. For example, values for material "Type 2" at 19.0 GHz was obtained by averaging the material values for "Type 1" and "Type 3" at 19.0 GHz. Thus, we effectively used 19 types of materials. For lossless layers, small values of losses were added, as it is practically not feasible to make a perfectly lossless dielectric. The first layer loss was usually 0.01 if it was selected lossless and for all other layers, the loss value was kept at 0.1 if lossless. Seven cases were attempted as follows.

- Case 1) Normal incidence ($\theta = 0.0$, $\phi = 0.0$), TE polarization.
- Case 2) Oblique incidence ($\theta = 45.0$, $\phi = 0.0$), TE polarization.
- Case 3) θ varying from 0° to 45°, TE polarization.
- Case 4) Normal incidence ($\theta = 0.0$, $\phi = 0.0$), TM polarization.
- Case 5) Oblique incidence ($\theta = 45.0$, $\phi = 0.0$), TM polarization.
- Case 6) θ varying from 0° to 45°, TM polarization.
- Case 7) θ varying from 0° to 45°, TE and TM polarization.

The population size and number of generations were fixed at 50 and 405, respectively. The periodicity of the FSS screen in the x- and y-directions were made equal. The loss in the FSS screen material was restricted to real values by forcing the imaginary part to be zero and the GA optimized at a frequency resolution of 1.0 GHz. To get the values of reflection coefficients at intermediate frequency points, a spline interpolation in frequency was done using MATLAB. The optimized parameters from the GA output were used in a separate code, which handled FSS screens embedded in lossy dielectric media. To verify the intermediate values of reflection coefficients, the FSS code was run at the same frequency resolution as the spline interpolation. If the reflection coefficient values at the intermediate frequencies generated by these two methods differed, the GA was rerun at a finer frequency resolution, using the population of the last generation, to obtain the correct values. The reflection coefficient in decibels is plotted versus frequency in Figs. 6–14 (all dimensions are in millimeters). In the FSS cell structure, white represents metal and black free space and symmetry along the y-axis is clearly observed in the FSS cell structures for all the seven cases. Table III lists the parameters selected by the GA

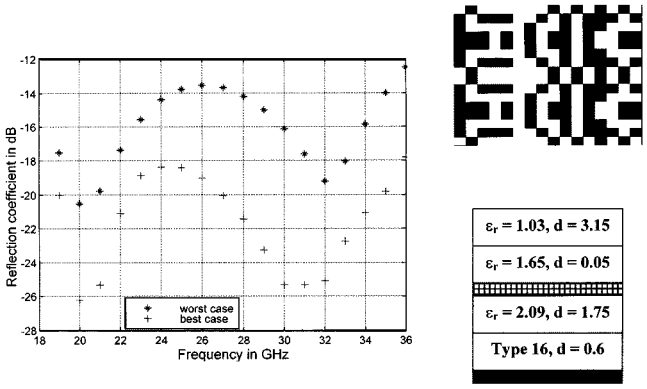

Fig. 8. Oblique incidence ($\theta = 0.0$ to 45.0, $\phi = 0.0$), TE polarization.

for each case. For all seven cases, the azimuthal angle was fixed at 0° ($\phi = 0.0$, x-z-plane).

It is observed in Figs. 6, 7, 10, and 11 that the frequency response obtained by using the GA resembles, as expected, the familiar filter response obtained by Chebyshev equal-ripple optimization procedures. For all the four cases, the worst-case reflection coefficient is maintained below −18.0 dB. In Figs. 8 and 12, the worst- and best-case reflection coefficients can be explained as follows. For a single frequency, over the elevation angles of interest ($\theta = 0.0$ to 45.0°), the maximum and minimum values of reflection coefficients correspond to the worst- and the best-cases of reflection-coefficient values in decibels. The additional burden of optimizing over a range of elevation angles results in the degradation of the worst-case reflection-coefficient value. Figs. 9(a)–(d) and 13(a)–(d) show the variation of the reflection coefficient as a function of the elevation angle with frequency as a parameter for the TE and TM polarization, respectively. Fig. 14 shows the worst- and best-case reflection coefficients obtained by the GA optimizing for TE and TM polarizations simultaneously over the elevation angles of interest ($\theta = 0.0$ to 45.0°). The worst-case reflection coefficient in this case was maintained below −15.0 dB. Figs. 15 and 16(a)–(c), illustrate certain details of the GA optimization procedure for case 7 as a representative example. Fig. 15 shows the variation in fitness value as given by (1) versus the number of generations. The following two important observations can be made from this curve: 1) the MGA restarts the population (as explained in Section II) at the 50th generation, as seen from the sudden dip in the curve for average fitness value and 2) the best value of

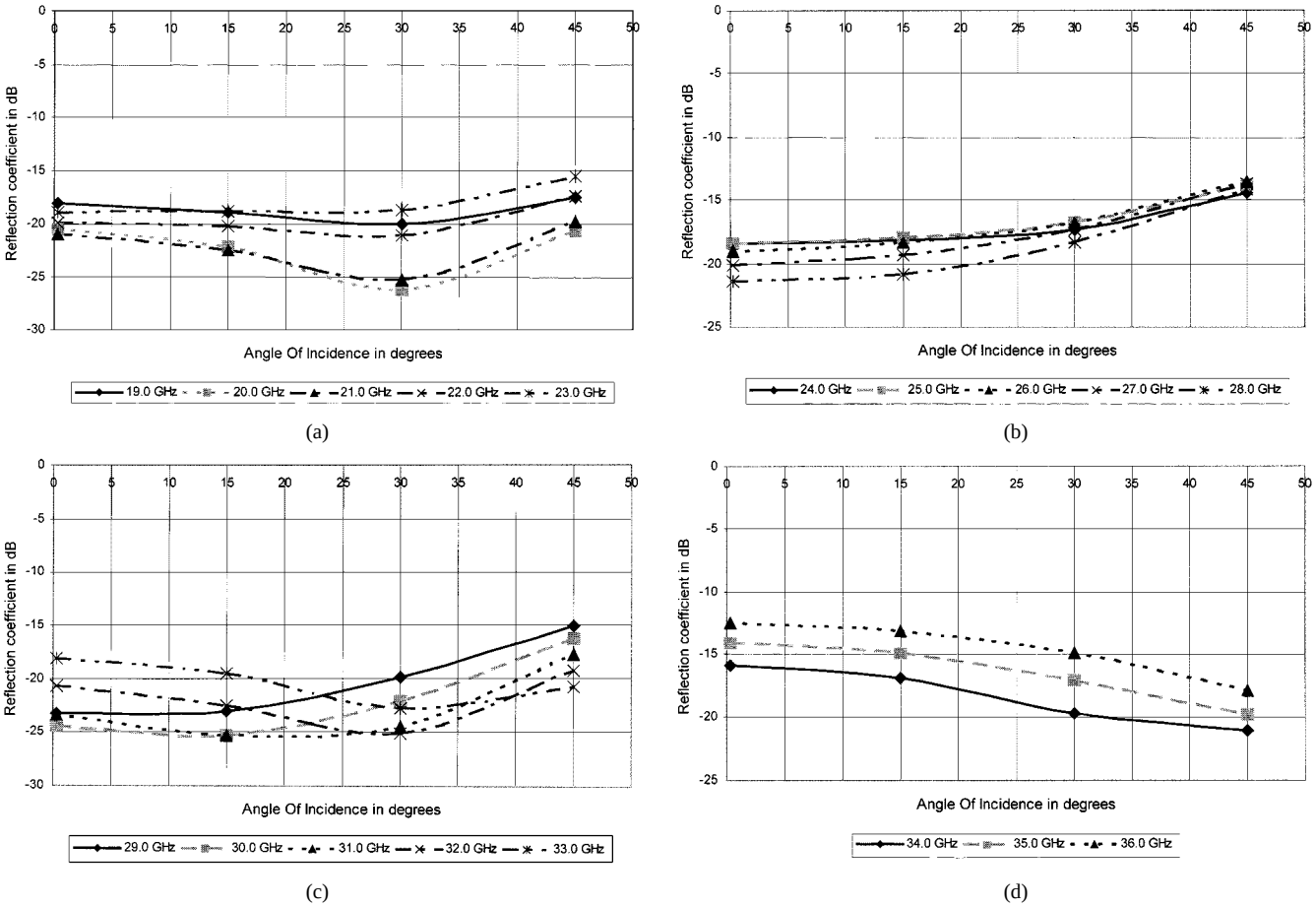

Fig. 9. Reflection coefficient as a function of elevation angle for TE polarization. (a) 19.0–23.0 GHz. (b) 24.0–28.0 GHz. (c) 29.0–33.0 GHz. (d) 34.0–36.0 GHz.

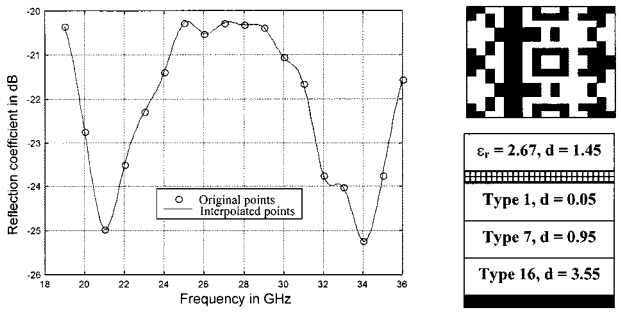

Fig. 10. Normal incidence, TM polarization.

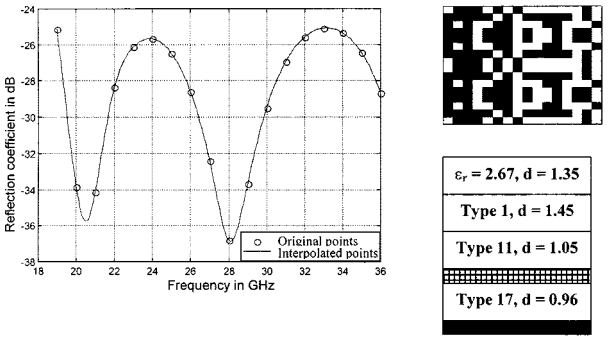

Fig. 11. Oblique incidence ($\theta = 45.0,\ \phi = 0.0$), TM polarization.

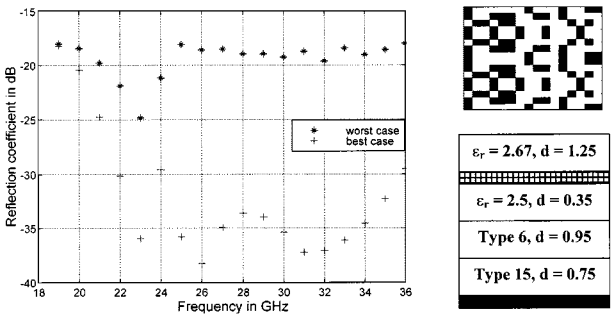

Fig. 12. Oblique incidence ($\theta = 0.0$ to 45.0, $\phi = 0.0$), TM polarization.

fitness (which is not necessarily the global maximum, but satisfies our design requirements) is reached by the 75th generation. Fig. 16 shows the population distribution at the 1st, 40th, and 75th generations, respectively.

Table IV shows the search space of the GA parameters for this problem. The number of these parameters is 18 if the MGA selects a PEC FSS screen and lossy dielectric layers, and the corresponding chromosome consists of 168 bits. However, if the MGA selects a lossy FSS screen and lossless dielectric layers, the number of parameters increases to 19 and the chromosome length is 194 bits. These two cases constitute the best- and worst-case scenarios in terms of population sizes for

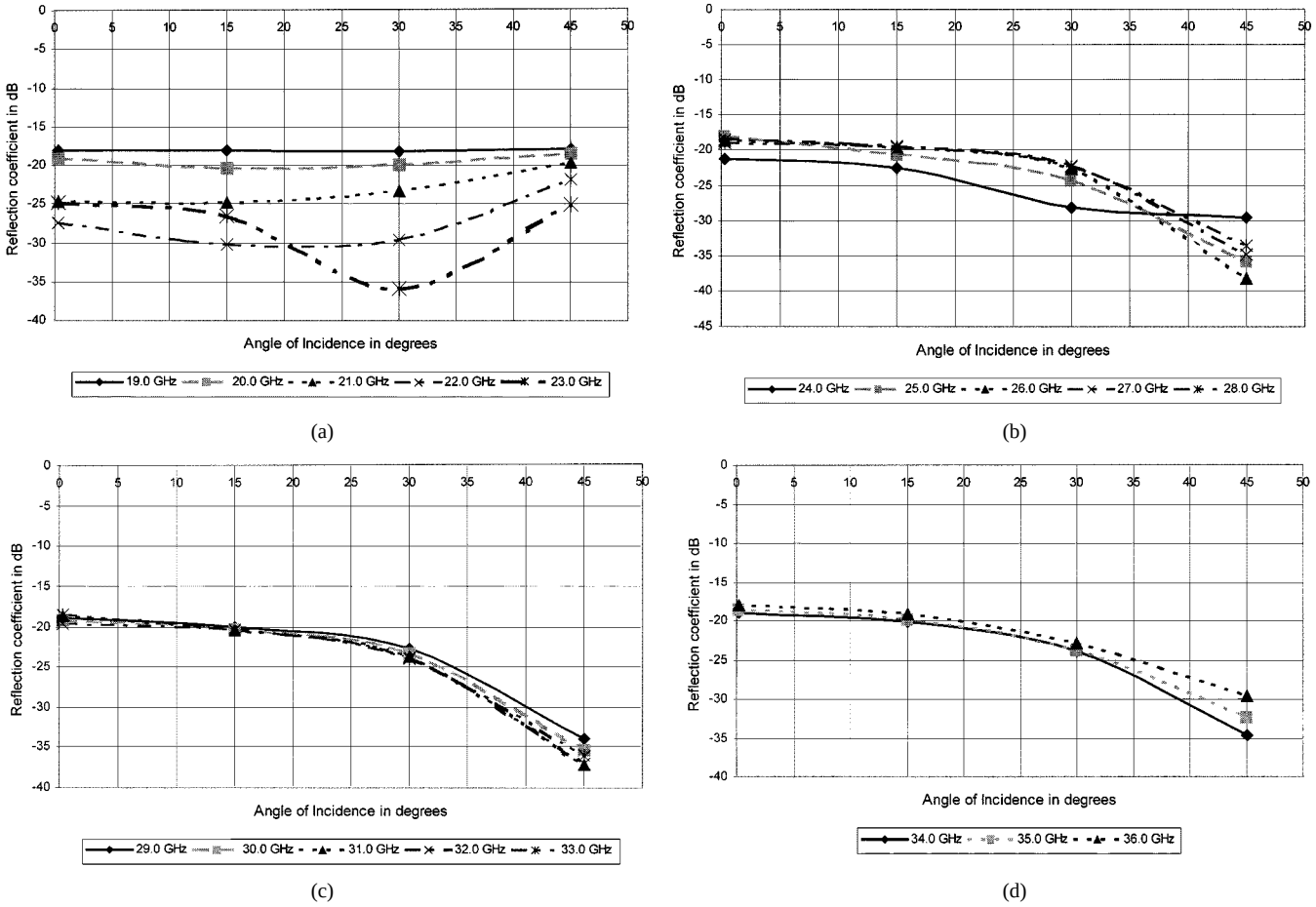

Fig. 13. Reflection coefficient as a function of elevation angle for TM polarization (a) 19.0–23.0 GHz. (b) 24.0–28.0 GHz. (c) 29.0–33.0 GHz. (d) 34.0–36.0 GHz.

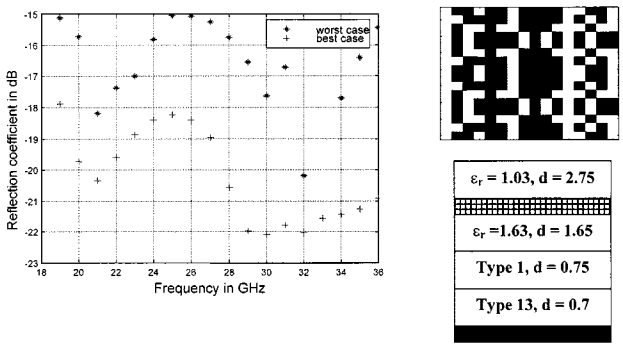

Fig. 14. Oblique incidence ($\theta = 0.0$ to 45.0, $\phi = 0.0$), TE and TM polarization.

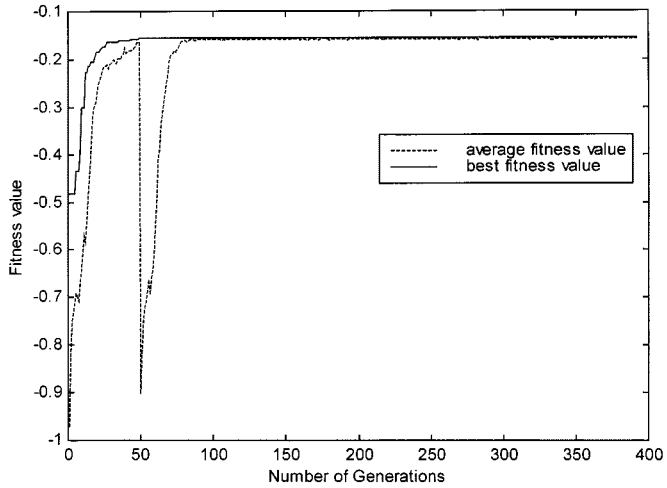

Fig. 15. Fitness value versus the number of generations for case 7.

the problem at hand. An estimate of the population size for a conventional GA can be derived from [3], [6]

$$n_{\text{pop}} = \left[\left(\frac{1}{k}\right)\chi^k\right] \tag{16}$$

where l is the length of the chromosome string, k is the size of the schema of interest, and χ is the number of possibilities for each bit or cardinality, which is two for binary coding. For the purpose of estimating an appropriate population size, it is assumed that each parameter string represents one important schema; therefore, the schema length is assumed to be equal to the average parameter length for estimation purposes. From Table IV, we see that, for the best case, we have $l = 168$, $\chi = 2$, and the average length of the schema of interest was $(1/18)(64+10+52+18+2+1+1+20) = 9$ (this is the average length of the number of chromosomes that make up one parameter), while for the worst case, the corresponding parameters were $l = 194$, $\chi = 2$, and the average length of the schema of interest was $(1/19)(64+10+52+18+2+1+10+1+36) = 10$. Applying (15), the population sizes for the best and worst cases can be estimated to be 9560 and 19866, respectively. Comparing the required population sizes for the MGA and the conventional

TABLE III
PARAMETERS SELECTED BY THE GA FOR THE SEVEN CASES

	Dielectric Layer types				FSS screen properties		
	Layer 1	*Layer 2*	*Layer 3*	*Layer 4*	*Position between*	*Cell size (mm)*	*Loss (Ω)*
Case 1	Lossless	Lossless	Lossy	Lossy	3rd and 4th	17.11 x 17.11	137.08
Case 2	Lossless	Lossless	Lossy	Lossy	3rd and 4th	11.26 x 11.26	164.45
Case 3	Lossless	Lossless	Lossless	Lossy	2nd and 3rd	11.16 x 11.16	394.16
Case 4	Lossless	Lossy	Lossy	Lossy	1st and 2nd	9.92 x 9.92	988.5
Case 5	Lossless	Lossy	Lossy	Lossy	3rd and 4th	31.78 x 31.78	646.36
Case 6	Lossless	Lossless	Lossy	Lossy	1st and 2nd	26.70 x 26.70	980.67
Case 7	Lossless	Lossless	Lossy	Lossy	1st and 2nd	8.767 x 8.767	447.93

TABLE IV
GA PARAMETER SEARCH SPACE

Parameters	Number of parameters	Range of parameters	Step size	Number of possibilities (nearest 2^n)	Number of binary digits
One row Total 4 rows	4	0 – 65535	1	65536	16 bits x 4 rows = 64
Total thickness of composite (mm)	1	0.1 – 6.0	0.01	1024	10
d_1, d_2, d_3, d_4	4	0.05 – 6.0	0.001	8192	13 bits x 4 layers = 52 bits
Tx_1, Ty_1	2	1.0 – 50.0	0.1	512	9 bits x 2 = 18 bits
FSS position	1	1 – 4	1	4	2
Choice of FSS screen material	1	1 – 3	1	2	1
$Re(Z_s)$	1	10.0 – 1000.0	1	1024	10
Choice of layer 1 material	1	1.0 – 3.0	1	2	1
ε_{r1}, ε_{r2}, ε_{r3}, ε_{r4} for lossless dielectric	4	1.03 – 6.0	0.01	512	9 bits x 4 layers = 36
Lossy dielectric for all four layers	4	1 – 19	1	32	5 bits x 4 layers = 20
Lowest total parameters	18			Lowest total bits = 168	
Highest total parameters	19			Highest total bits = 194	

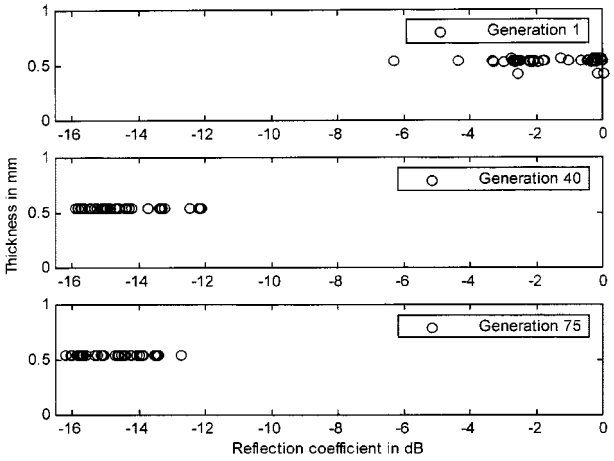

Fig. 16. Population distribution of the GA in the 1st, 40th, and 75th generations.

GA, we see that the employment of the former in optimizing the design problem in this paper is justified. It is clearly evident that the savings in computational time and resources over the conventional GA are substantial when the MGA is used.

V. CONCLUSIONS

A novel approach, which is based on a binary-coded GA, has been developed to optimize a broad-band microwave absorber, which employs FSS screens embedded in dielectric media. Given the total number of dielectric layers, the total thickness of the composite, and the range of permittivity values for each layer, the GA iteratively constructs a composite whose frequency response closely matches the desired response. The GA also optimizes the FSS cell design, its x- and y-periodicities, its position within the dielectric composite, and the loss value of the FSS screen, as appropriate. The major advantage of the

present approach is that it is simple and that it demands far less computational time and resource than does the conventional GA to solve the same problem. We have shown that the MGA technique can successfully handle multidimensional and multimodal optimization problems by using small population sizes, which gives it an edge over conventional GAs. All of the designs presented in this paper were run on a DEC-ALPHA 500 workstation, which employed a machine optimized math library specially designed for the LAPACK subroutines used to invert the FSS–MoM matrix. Cases 1, 2, 4, and 5 took about 8 h to complete. The increase in computation time for cases 3 and 6, which took about 15 h to complete, can be attributed to the additional optimization with respect to the elevation angles. Case 7 had the greatest run time (about 24 h), and this is because it required simultaneous optimization with respect to polarization and elevation angles.

ACKNOWLEDGMENT

The authors gratefully acknowledge the technical support provided by Dr. J. F. Ma, Electromagnetic Communication Laboratory, Pennsylvania State University, University Park, in implementing the LAPACK subroutines and increasing the computational efficiency of the program. The authors are also grateful to W. L. Gore and Associates Inc., Newark, DE, for providing the measured values of the frequency-dependent material parameters.

REFERENCES

[1] J. M. Johnson and Y. Rahmat-Samii, "An introduction to genetic algorithms," in *Electromagnetic Optimization by Genetic Algorithms*, Y. Rahmat-Samii and E. Michielssen, Eds. New York: Wiley, 1999, pp. 1–27.

[2] D. S. Weile and E. Michielssen, "Genetic algorithm optimization applied to electromagnetics: A review," *IEEE Trans. Antennas Propagat.*, vol. 45, pp. 343–353, Mar. 1997.

[3] D. E. Goldberg, K. Deb, and J. H. Clark, "Genetic algorithms, noise, and the sizing of populations," in *Complex Systems*. Urbana, IL: Complex Syst., vol. 6, pp. 333–362.

[4] D. E. Goldberg, "Sizing populations for serial and parallel genetic algorithms," Clearinghouse Genetic Algorithms, Univ. Alabama, Akron, AL, TCGA Rep. 88 004, 1988.

[5] K. Krishnakumar, "Micro-genetic algorithms for stationary and nonstationary function optimization," in *SPIE: Intelligent Control and Adaptive Systems*. Philadelphia, PA: SPIE, 1989, vol. 1196.

[6] D. L. Carroll, "Genetic algorithms and optimizing chemical oxygen–iodine lasers," in *Developments in Theoretical and Applied Mechanics*, H. Wilson, R. Batra, C. Bert, A. Davis, R. Schapery, D. Stewart, and F. Swinson, Eds. Akron, AL: School Eng., Univ. Alabama, 1996, vol. XVIII, pp. 411–424.

[7] D. E. Goldberg and K. Deb, "A comparative analysis of selection schemes used in genetic algorithms," in *Foundations Of Genetic Algorithms*, G. J. E. Rawlins, Ed. San Mateo, CA: Morgan Kaufmann, 1991, pp. 69–93.

[8] J. M. Johnson and Y. Rahmat-Samii, "Genetic algorithms in electromagnetics," in *Proc. IEEE Int. AP-S Symp. Dig.*, Baltimore, MD, 1996, pp. 1480–1483.

[9] R. Mittra, C. H. Chan, and T. Cwik, "Techniques for analyzing frequency selective surfaces—A review," *Proc. IEEE.*, vol. 76, pp. 1593–1615, Dec. 1988.

[10] C. G. Christodoulou and J. F. Kauffman, "On the electromagnetic scattering from infinite rectangular grids with finite conductivity," *IEEE Trans. Antennas Propagat.*, vol. AP-34, pp. 144–154, Feb. 1986.

[11] C. H. Tsao and R. Mittra, "A spectral-iteration approach for analyzing scattering from frequency selective surfaces," *IEEE Trans. Antennas Propagat.*, vol. AP-30, pp. 303–308, Mar. 1982.

[12] C. H. Chan, "Analysis of frequency selective surfaces," in *Frequency Selective Surfaces and Grid Array*. ser. Microwave Opt. Eng., T. K. Wu, Ed. New York: Wiley, 1995, pp. 27–86.

[13] T. Itoh, "Spectral domain immitance approach for dispersion characteristics of generalized printed transmission lines," *IEEE Trans. Microwave Theory Tech.*, vol. MTT-28, pp. 159–164, Mar. 1975.

Sourav Chakravarty (S'98) was born in West Bengal, India, in 1971. He received the Bachelors degree in electronics and communication from the Regional Engineering College, Kurukshetra, India, in 1992, the Masters degree in electronics and telecommunication from the Jadavpur University, Calcutta, India, in 1997, and is currently working toward the Ph.D. degree in electrical engineering at the Pennsylvania State University, University Park.

He is currently a Research Assistant in the Electromagnetic Communication Laboratory, Pennsylvania State University. His current research interests include computational electromagnetics, optimization techniques, and on/off chip interconnect analysis using the finite-difference time-domain (FDTD) technique.

Raj Mittra (S'54–M'57–SM'69–F'71–LF'96) is currently a Professor in the Electrical Engineering Department, Pennsylvania State University, University Park. He is also the Director of the Electromagnetic Communication Laboratory, which is affiliated with the Communication and Space Sciences Laboratory of the Electrical Engineering Department. Prior to joining Pennsylvania State University, he was a Professor in Electrical and Computer Engineering Department, University of Illinois at Urbana-Champaign. He is also the President of RM Associates, a consulting organization that provides services to industrial and governmental organizations both in the U.S. and abroad. For the last 15 years, he has directed, as well as lectured in, numerous short courses on computational electromagnetics, electronic packaging, and wireless antennas, both nationally and internationally. He was a Visiting Professor at Oxford University, Oxford, U.K., and at the Technical University of Denmark, Lyngby, Denmark. He has authored or co-authored over 500 journal papers and 30 books or book chapters on various topics related to electromagnetics, antennas, microwaves, and electronic packaging. He holds three communication antennas patents. His professional interests include the areas of communication antenna design, RF circuits, computational electromagnetics, electromagnetic modeling and simulation of electronic packages, electromagnetic compatibility (EMC) analysis, radar scattering, FSSs, microwave and millimeter-wave integrated circuits, and satellite antennas. He is currently the North American Editor of *AEÜ*.

Dr. Mittra is a Life Fellow of the IEEE. He was President of the IEEE Antennas and Propagation Society (IEEE AP-S) and was the editor of the IEEE TRANSACTIONS ON ANTENNAS AND PROPAGATION. He was the recipient of the 1965 Guggenheim Fellowship Award, the 1984 IEEE Centennial Meda, and the 2000 IEEE Millennium Medal.

Neil Rhodes Williams (S'95–M'95) received the B.S. degree in electrical engineering from Wilkes University, Wilkes-Barre, PA, in 1987, and the M.S. degree in electrical engineering and Ph.D. degree in engineering science and mechanics from Pennsylvania State University, University Park, in 1989 and 1994, respectively. His doctoral dissertation concerned the radiative transfer approach to the design of the electromagnetic response of microwave chiral composites.

In Fall 1987, he joined the Department of Electrical Engineering, Pennsylvania State University, where he was a Research Assistant involved with conducting polymers, RAM and electromagnetic interference (EMI) materials. During 1990 and 1994, he served as a Design and Development Engineer at Research Park, University of Pennsylvania, where he was involved with advanced electrical composites and electrical material characterization systems. From 1994 to 1996, he was an Engineer/Scientist in the field of global positioning system (GPS) ground systems for Lockheed Martin. During this time, he was involved with signal-processing techniques for atmospheric signal propagation, as well as new architecture development for GPSs. His research has included manipulation of GPSs in military arenas. In 1996, he joined W. L. Gore and Associates, Newark, DE, where he is currently an Engineering Director for advanced electromagnetic products, and is involved with flexible magnetic resonance imaging (MRI) surface coils for MRI scanner systems. His research responsibilities also include microwave and optical fabrics and electronic material characterization systems. Some products, which have precipitated from this research area, are radome and electromagnetic manipulating fabrics.